Voltage Estimation for Diode-Clamped MMCs Based on a Simplified Neural Network

Nima Tashakor, Davood Keshavarzi, Shady Banana, and Stefan Goetz
Technische Universität Kaiserslautern
Kaiserslautern, Germany
E-Mail: tashakor@eit.uni-kl.de

Acknowledgements

The authors acknowledge the financial support by the Federal Ministry of Education and Research of Germany in the project "Open6GHub" (grant number: 16KISK004).

Keywords

«Capacitor voltage balancing», « Estimation technique», «Modular converter», «Modular multilevel converter», «Neural network».

Abstract

The modular multilevel converter (MMC) is a popular solution in high-voltage dc application and has significant potential in others. Generally, the MMC's stable operation is at the expense of numerous sensors, communication burdens, and complicated balancing strategies that can suppress its expansion in to cost driven applications. Hence, the introduction of a sensorless voltage balancing strategy with a simple controller is an attractive objective. A diode-clamped MMC offers a simple and yet effective solution by providing a balancing path between two modules through a diode. However, to compensate the lack of bidirectional energy transfer, modifying modulation technique is necessary. The level-adjusted phase-shifted carrier (LA-PSC) modulation introduces a small circulating current that ensures a correct balancing direction. Although the open-loop implementation of LA-PSC might be necessary for cost reduction in some applications, protection and control considerations may still necessitate careful monitoring of the modules' voltages. This paper proposes a voltage estimation strategy based on a simple neural network that does not require any measurement of the modules' voltages. Provided analysis as well as the simulation results confirm that the estimator can track the voltages with above 99% accuracy during balanced and imbalanced conditions.

Introduction

The modular multilevel converter (MMC) is a promising solution for high-voltage applications. Its advantages compared to other multilevel converters are excellent harmonic cancellation through quantized voltage levels, simple scalability, and higher flexibility due to its modularity [1-3]. These advantages make MMCs distinctly appealing for medium- to high-voltage applications [4, 5]. However, there are still challenges that need to be addressed, in which balancing and monitoring functions are among the most critical ones [6-8].

Balancing of MMC modules is pursued through two approaches. The first approach is based on various sorting algorithms, which necessitate constantly measuring the modules' voltages and transmitting the measured values back to the central controller [9-11]. In this approach, direct measurements through multiple sensors at modules terminals as well as a high-bandwidth communication interface increase the cost and complexity of the system [12, 13]. The required cell-sorting procedure further reduces the appeal of these methods, while it complicates safety-critical functions [14, 15]. The second approach modifies the macro- and micro-structure of the MMCs to generate balancing paths between the submodules through parallel connections [16-21]. Such topology modifications have great potential to solve some of the main challenges of MMCs [8, 22-24]. Some

well-known examples of such topologies are MMCs with parallel mode [19, 25, 26], Marx MMC [27], and MMC with clamped switches [6, 28] are examples of auto-balancing topologies, which can achieve stable sensorless operation. However, most modifications require extra active switches and driving circuitry that although attractive in some applications, hinder the more widespread acceptance in high-voltage systems due to the cost or extra complexity [29, 30].

The diode-clamped module is the simplest configuration that does not need additional controlled semiconductors and can achieve self-balancing [31, 32]. In such circuits, one or more diodes form parallel connections between adjacent modules [27, 33-35]. Fig. 1 shows the simplest configuration of a diode-clamped topology with a single diode. Since the diode can only conduct in one direction, the formed balancing path will be unidirectional. However, there are other clamping topologies to create a physical bidirectional balancing path with more complex structures [27, 29, 32, 33]. This further complicates the topology and increase the cost [32].

Fortunately, there is a more practical approach to enforce a balancing direction that is compatible with the diode conduction path. This can be easily achieved by manipulating the modulation reference of each module. Liu et al. achieve this by constantly measuring voltage of the module at the highest end of each arm and constantly controlling its modulation index [34]. While this method is inherently interesting, it requires constant measurement of the voltage and will also change the shape of the arm voltage. Zheng et al. control the balancing direction by introducing different delays in switching functions of different modules, i.e., the higher the module is positioned in the arm, the higher its corresponding delay [29]. Since the method is open-loop, it can reduce the balancing efficiency due to overcompensation. In addition, the delays can change the shape of the output voltage. We proposed a simple open-loop balancing method that adjusts the vertical starting point of the carriers, the so called level-adjusted phase-shifted carrier (LA-PSC) modulation [36]. Even though LA-PSC does not change the output voltage shape, it may suffer from overcompensation in certain conditions which can be critical in some applications.

Although there are various sensorless and open-loop balancing approaches, knowing the modules' voltages are vital due to monitoring and protection concerns [37-41]. Therefore, this paper proposes estimation based on a simplified neural network for diode-clamped MMC with LA-PSC modulation. The proposed method benefits from simplicity and does not require any voltage measurement at module levels, which leads to minimizing communications and cost.

Diode-clamped MMC

Fig. 1 illustrates the single-phase diode-clamped MMC topology consisting of two similar arms. The

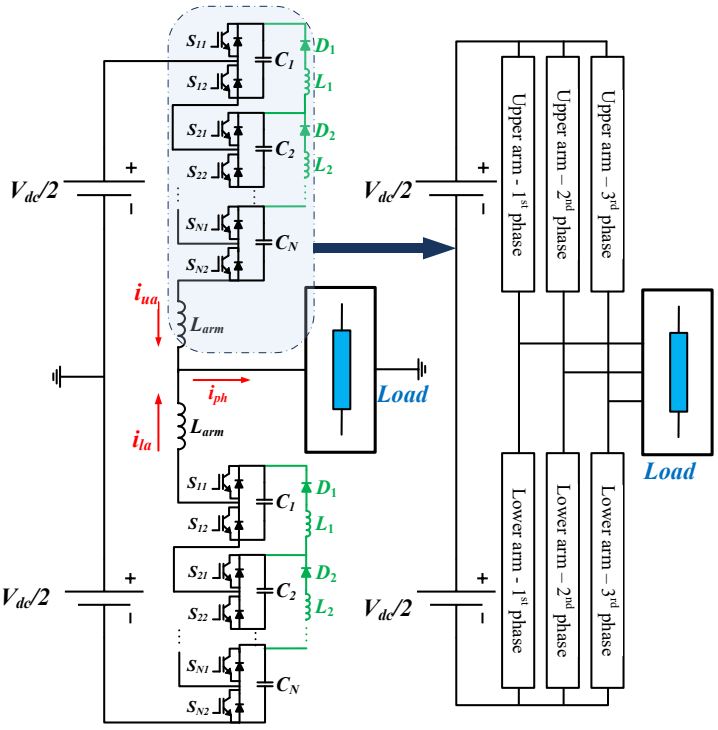

Fig. 1: single and three-phase topology of diode-clamped MMC

three-phase system can be easily developed based on single-phase topology.

Operation of the clamping circuit

In MMC, each arm contains N modules with $(N-1)$ clamping circuits, which consists of a diode and an inductor in series. The inductor restricts the maximum balancing current to protect the diode from large currents. The voltage across the clamping branch (v_{b_i}) includes the diode voltage (V_{fd}) and the inductance voltage (v_{L_i}) as well as the voltage across the total resistance of the path ($v_{R_{sum}}$) per

$$v_{b_i} = V_{\mathrm{fd}} + v_{L_i} + v_{R_{sum}}. \quad (1)$$

Depending on the control signal of the $(i+1)^{\mathrm{th}}$ module, we have three possibilities for the module voltage. When $S_{(i+1)1}: off$ and $S_{(i+1)2}$:on, voltage across the clamping branch is $v_{b_i} = v_{c_{i+1}} - v_{c_i}$. If $v_{c_{i+1}}$ is smaller than $v_{c_i} + V_{\mathrm{fd}}$, the diode is open as Fig. 2(a) shows, but if $v_{c_{i+1}}$ is larger than $v_{c_i} + V_{\mathrm{fd}}$, a balancing current flows from C_{i+1} to C_i as Fig. 2(b) illustrates. When $S_{(i+1)1}: on$ and $S_{(i+1)2}: off$ and the diode is reverse biased, and the balancing current declines to zero as Fig 2(c) depicts and remains zeros as the diode cannot conduct in reverse. With negligible resistive elements ($V_{R_{sum}} = 0$), the derivative of the clamping inductors is

$$\frac{\mathrm{d}i}{\mathrm{d}t} = \frac{-\left(v_{c_i} + V_{fd}\right)}{L_i}. \quad (2)$$

In the case of large imbalances between two modules, multiple switching sequences are necessary,

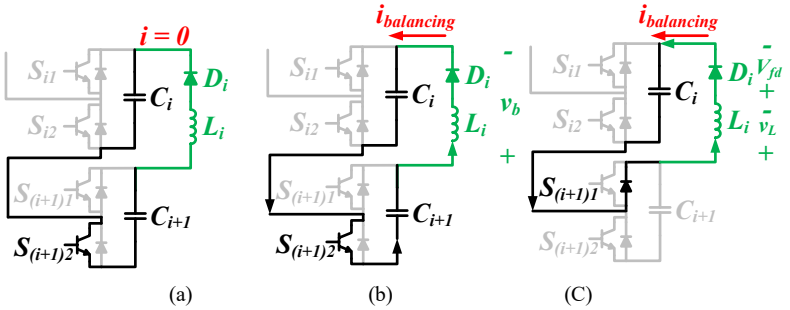

Fig. 2. Different operation modes of the diode-clamped modules

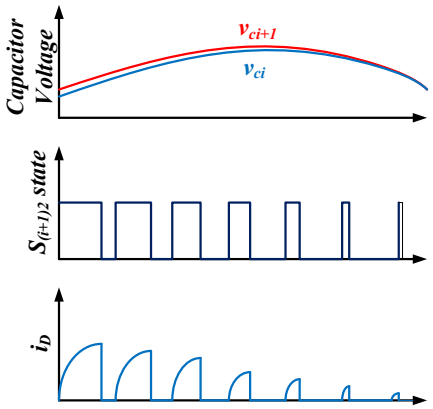

Fig. 3: Balancing process for two adjacent modules

until the voltage difference of the modules becomes negligible ($v_{c_{i+1}} - v_{c_i} \leq V_{\mathrm{fd}}$). Fig. 3 shows an intuitive representation of this procedure. Therefore, ignoring of the initial voltage of each module, the final relation between the $v_{c_{i+1}}$ and v_{c_i} would be $v_{c_i} + V_{\mathrm{fd}} > v_{c_{i+1}}$. The analysis can be extended to all the modules in an arm following

$$v_{c_1} + V_{\mathrm{fd}} \geq \ldots \geq v_{c_{(N-1)}} + V_{\mathrm{fd}} \geq v_{c_N}. \quad (3)$$

Circuit analysis

Fig. 4(a) shows the equivalent electrical circuit when $S_{(i+1)2}$ is on (forward-bias state) and $V_{c_{i+1}} > V_{c_i} + V_{fd}$, where R_{L_i} represents the internal resistance of the inductance L_i, and $R_{C_{i+1}}$ as well as R_{C_i} are

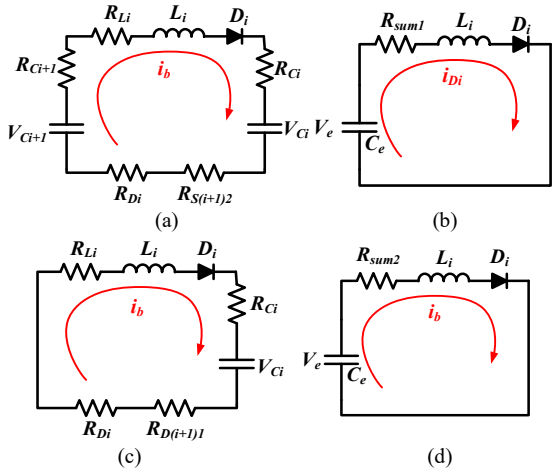

Fig. 4. Electrical circuit during the balancing: (a) $S_{(i+1)2}$ is on and balancing current flows from C_{i+1} to C_i; (b) simplified electrical circuit when $S_{(i+1)2}$ is on; (c) $S_{(i+1)2}$ turns off and balancing current decays to zero; (d) simplified electrical circuit when $S_{(i+1)2}$ is off.

the internal resistances of the capacitors C_{i+1} and C_i. Similarly, $R_{S_{(i+1)2}}$ is the internal resistance of the switch $S_{(i+1)2}$. Additionally, Fig. 4(b) depicts the simplified electrical circuit, V_e is the equivalent voltage, and C_e is the equivalent capacitance. According to the simplified electrical circuit, the total branch resistance $R_{\text{sum1}} = R_{C_{i+1}} + R_{L_i} + R_{C_i} + R_{S_{(i+1)2}}$, the equivalent voltage $V_e = V_{c_{i+1}} - V_{c_i}$, and the equivalent capacitance $C_e = 0.5C_i = 0.5C_{i+1}$ and the resulted second order RLC circuit can be readily analyzed. When $S_{(i+1)2}$ turns off, the electrical circuit changes to Fig. 4(c). Similarly, Fig. 4(d) shows the simplified electrical circuit in this mode, where $V_e = V_{c_i}$, $C_e = C_i$, and $R_{\text{sum2}} = R_{L_i} + R_{C_i} + R_{S_{(i+1)1}}$. Based on Kirchhoff voltage law in Fig. 4(b) and after some manipulations a second-order differential equation can be derived as follows

$$\frac{\mathrm{d}^2 i_D(t)}{\mathrm{d}t^2} + \frac{R_{\text{sum1}}}{L_i}\frac{\mathrm{d}i_D(t)}{\mathrm{d}t} + \frac{1}{L_i C_e} i_D(t) = 0 \tag{4}$$

Applying Laplace transformation and solving it arrives to

$$P_{1,2} = -\frac{R_{\text{sum1}}}{2L} \pm \sqrt{\frac{{R_{\text{sum1}}}^2}{4L_i^2} - \frac{1}{L_i C_e}} \tag{5}$$

The equivalent resistance $R_{sum1}$is relatively small, $R_{\text{sum1}} < 2\sqrt{\frac{L_i}{C_e}}$, hence with normal parameters the current will have a damped oscillation given by

$$i_D(t) = \frac{U_{\text{diff}}}{\sqrt{\frac{L_i}{C_e} - \frac{{R_{\text{sum1}}}^2}{4}}}\, e^{-\alpha t} \sin \omega_d t \tag{6}$$

where the damping factor $\alpha = \frac{R_{\text{sum1}}}{2\,L_i}$, and the frequency of the oscillation is $\omega_d = \sqrt{\frac{1}{L_i C_e} - \frac{{R_{\text{sum1}}}^2}{4L_i^2}}$. Furthermore, it should be noted that the clamping path only allows for the current to pass in one direction, and the current cannot be negative.

If the maximum permissible voltage difference between modules is $U_{\text{diff\_max}}$, the maximum peak diode current I_{Pmax} follows

$$I_{\text{P\_max}} = \frac{U_{\text{diff\_max}}}{\sqrt{\frac{L_i}{C_e} - \frac{{R_{\text{sum1}}}^2}{4}}}. \tag{7}$$

Therefore, selecting the inductor per

$$L_i \geq \left(\frac{{R_{\text{sum1}}}^2}{4} + \frac{{U_{\text{diff\_max}}}^2}{{I_{\text{P\_max}}}^2}\right) C_e, \tag{8}$$

ensures that the current of the clamping diode (D_i) is below its rated value [34]. Further reduction of the current rating of the diode is possible by increasing the size of the clamping inductor. However,

larger inductor values reduces the speed of balancing [42]. A more detailed design procedure for the clamping diode and inductor are provided in the literature [36].

Level-Adjusted Phase-Shifted Carrier (LA-PSC)

The conventional phase-shifted carrier (PSC) modulation compares a reference waveform (modulation index) with carriers that are phase-shifted with respect to each other. In PSC modulation, each carrier corresponds to one unique module in the arm and the phase-shift between two successive carriers is fixed to $\frac{2\pi}{N}$. With ideal conditions, PSC should reach a stable operating point, but in practice, the system gradually diverges from the desired operation point unless balancing mechanism exists [24].

A diode-clamped circuit can guarantee that condition (3) is always preserved, and the LA-PSC modulation can ensure the correct balancing direction by a small vertical displacement in the conventionally inline carriers. Fig. 5 illustrates an intuitive representation of the shifted carriers in LA-PSC modulation. A positive level-adjustment (for the i^{th} carrier, $\delta_i > 0$) decreases the average duration that the module is connected in series and a negative level-adjustment ($\delta_i < 0$) increases the average duration of series intervals. Lower duration with series connection reduces the module charge and vice versa due to positive average arm current. If δ_i is the vertical-adjustment of i^{th} carrier, $\delta_1 \geq \delta_2 \geq \cdots \geq \delta_N$ ensures a bottom to top balancing direction at all times. The effective modulation index (m_i) for the i^{th} module in upper arm with a level-adjustment equal to δ_i is

$$m_{u,i} = \frac{1-m_a \sin(\omega t)}{2} - \delta_{u,i}, \tag{9}$$

where m_a is the normalized amplitude of the phase a.

Since the modulation index of each module is controlled separately, it is possible to directly control the modulation indexes per (9) with similar results regarding the balancing direction. The effective modulation index for the complete arm is the average of all the individual m_i values as

$$m_u = \frac{1-m_a \sin(\omega t)}{2} - \frac{\sum_i^N \delta_{u,i}}{N}. \tag{10}$$

Defining the level-adjustments for the i^{th} module in the upper arm per

$$\delta_{u,i} = \Delta_a \left(\frac{1}{2} - \frac{j-1}{N-1}\right) \tag{11}$$

results in a zero average for the term corresponding to the level-adjustment in (10), and hence an unchanged effective voltage of the arm. Δ_a in (11) is the total level-adjustment between the first and last carriers of the arm.

Since the balancing direction in the lower arm must also be from bottom to top, $\delta_{l,i}$ should be equal to

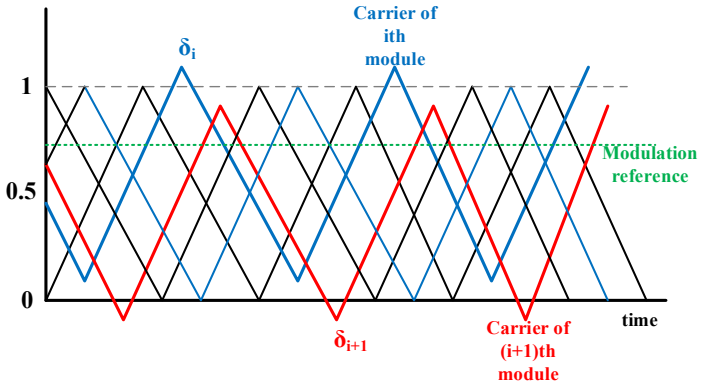

Fig. 5. Intuitive representation of the PSC and the LA-PSC

$\delta_{u,i}$ following (11). However, the phase-shifts' of the carriers in the upper and lower arm should be mirrored, (i.e., the phase-shift of the first module in the upper arm should be equal to the phase-shift of the last module in the lower arm) to cancel out the effects of the phase level-adjustments on the phase voltage, e.g., vector of phase-shifts for the upper and lower arm can be $\phi_u = \left[0, \frac{2\pi}{N}, \ldots, \frac{2\pi(N-1)}{N}\right]^T$ and $\phi_l = \left[\frac{2\pi(N-1)}{N}, \frac{2\pi(N-2)}{N}, \ldots, 0\right]^T$. Therefore, the new carriers for the upper and lower arms, respectively, are

$$C_{u,i}^{\text{new}} = \Delta_a(\frac{1}{2} + \frac{j-1}{N-1}) + C_{u,i}^{\text{old}}, \quad (12)$$

$$C_{l,i}^{\text{new}} = \Delta_a(\frac{1}{2} + \frac{j-1}{N-1}) + C_{l,N-i}^{\text{old}}. \quad (13)$$

Proposed estimation algorithm

Although, the behavior of the diode-clamped MMC is easy to understand, obtaining accurate analysis considering all the inherent dynamics is challenging. Furthermore, the non-uniform distribution of the mismatches among modules as well as the effect of the proposed level-adjustments would make a detailed analytical solution even more difficult or even unfeasible.

On the other hand, some methods based on machine learning such as neural network (NN) do not suffer from such restrictions. The random nature of parameter tolerances (e.g., self-discharge of the modules) makes deriving a mathematical solution almost impossible while it be easily modelled through proper training of the NN. Furthermore, accurate analytical solutions are challenging, but it is possible to define the output boundaries for each of the module voltages as corrective measures in case a NN starts to deviate from normal behavior.

Proposing a new NN is not the purpose of this paper, and to reduce the computational burden, as an example, the simplest form of a neural network estimates the voltage of the modules. The back propagation (BP) algorithm is selected to train this network. Additionally, a boundary function checks the fidelity of the NN's output.

The main idea of the BP algorithm is to choose the weights of the neural network (NN) in a manner that the error between the desired output and the NN output can be minimized. The method for minimizing the error is based on the gradient descent approach. The NN is responsible for minimizing the error between the estimation of the output voltage and its measurement based on the module states. The output voltage of the arm respecting to the module voltages and their states is

$$V_{arm} = \sum_{j=1}^{N} V_{c_j} S_{j1} = \boldsymbol{V_c^T} \times \boldsymbol{S_1} \quad (14)$$

where $\boldsymbol{V_c}$ is the vector of module voltages in one arm and $\boldsymbol{S_1}$ is the vector of the upper switches (S_{j1}) in each module in the same arm.

As Fig. 6 illustrates, the NN is composed of one input vector (module states), one layer with one neuron (representation of single equation for one arm), and one output (arm voltage). Each element of input vector of the NN ($\boldsymbol{X}(k)$) is the switching signal of one module in the arm, $X_j(k) = S_{j1}$, per

$$\boldsymbol{X}(k) = [S_{11} \quad S_{21} \quad \cdots \quad S_{N1}], \quad (15)$$

where $S_{j1} = 1$ and $S_{j1} = 0$, respectively, if the j^{th} module is connected in series or if it is bypassed.

The desired output is the arm voltage $d = \text{y}(k)$, which is already measured for higher level controls, and the weighting vector represents the estimated voltage of the modules $\boldsymbol{W}(k) = \boldsymbol{V_{c,est}}$ at the k^{th} step per

$$\boldsymbol{W}(k) = \left[V_{c_1,est} \quad V_{c_2,est} \quad \cdots \quad V_{c_N,est}\right]. \quad (16)$$

A linear activation function, $f(\alpha) = \alpha$, simplifies implementing the BP algorithm. Therefore, the derivative of the activation function is $f'(\alpha) = 1$. Table I shows the pseudo-code of the BP algorithm. Hence, the BP will determine the best weights (modules' voltages) that reduce the error between the estimated and measured arm voltage. As an improvement to the BP algorithm a momentum term can be used for updating the weights per

$$\Delta w_j(k) = \eta \left((1-\alpha)\delta x_j(k) + \alpha \Delta w_j(k-1)\right), \quad (17)$$

where α is a momentum constant in the range $0 \leq \alpha < 1$ and η is the learning rate. The momentum term reduces the oscillations in the beginning of the estimation. The value of the learning rate (η) influences the learning behavior, i.e., small η values can slow the convergence, and with large η values can cause oscillation and/or even divergence. Although η and α are normally defined heuristically, they depend on the switching frequency of the modules as well as the sampling frequency. We have selected $\eta = 0.001$ and $\alpha = 0.1$.

Table. I: Pseudo-code of the estimtor based on BP

STEP 0	Initialization of the weights	$w_j = V_{\mathrm{c_j},est}\ ,\ \mathrm{j} = 1, \ldots N$
STEP 1	Compute the output ($\hat{y}$)	$\hat{y} = f(\alpha) = \alpha = X(k) \times \mathrm{W}(k)$
STEP 2	Compute the error	$e = y(k) - \hat{y}$
STEP 3	Compute the local gradients	$\delta = f'(\alpha)e$
STEP 4	Compute the weight updates	$\Delta w_j = \eta\ \delta\ \mathrm{x_j}(k)$
STEP 5	Compute the new weights	$w_j(k) = w_j(k) + \Delta w_j$
STEP 6	Return to	STEP 1

Simulation results

A single-phase configuration with 16 modules ($N = 8$) and 14 clamping branches verifies the feasibility of the proposed estimation technique. Table. II lists the parameters of the simulation systems. The switching frequency of each module is selected to be 5 kHz, which results in the equivalent switching frequency of 40 kHz for each arm.

Table. II: Parameters of the Simulation and Experimental Setups

Parameters		Simulation
Rated Power		$P_{ac} = 1.14$ MW
Load Inductor		$L_L = 0.1$ mH
Module rated voltage		$V_{sm} = 1.2$ KV
DC link voltage		$V_{dc} = 9.6$ KV
Number of the modules		16
Arm inductance		$L_{arm} = 5$ mH
Arm Resistor		$R_{larm} = 50$ mΩ
Carrier frequency		$f_c = 5$ KHz
Sampling frequency		$f_s = 0.1$ MHz
Output frequency		$f = 50$ Hz
Modules	Capacitance	$C_{cap} = 6$ mF
	Capacitor resistor	$R_{cap} = 2$ mΩ
Modulation index		$m = 0.75 \sim 0.95$
Clamping Circuit	Inductance	$L_{ld} = 10$ µH
	Resistor	$R_{ld} = 0.5$ mΩ

We study the behavior of the estimator under balanced conditions with identical modules and imbalanced conditions with mismatch between module capacitances and self-discharge rates. The estimator is initialized to random values to show that the estimator is stable and can converge even with completely incorrect initial values, however, the steady-state voltages of the modules can be also used for initialization. Fig. 7 studies the behavior of the proposed estimator during balanced condition. As seen, the real voltages of modules have variation around the nominal voltage in and the estimator follows them properly. The estimation accuracy is above 99% and it converges in less than 50 ms. Fig. 8 illustrate the estimator behavior in an imbalanced system caused by inserting a parallel resistor

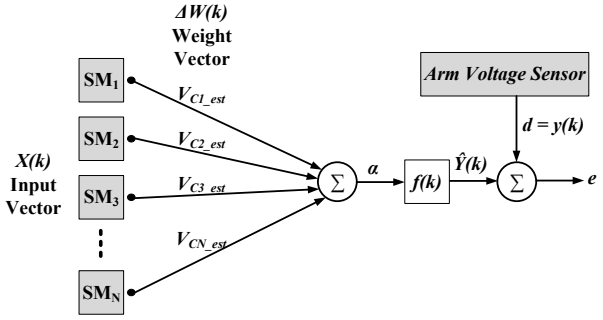

Fig. 6: Different operation modes of the diode-clamped modules

(about a few hundred ohms) with the third module. As shown in Fig. 8, the proposed algorithm can estimate the modules' voltages with above 99% accuracy. In both scenarios, the estimator closely follows the module voltages and can achieve above 99% accuracy, which further verify the capability of the proposed estimator.

Conclusion

This paper proposes an estimator based on a simplified NN that can be integrated into the control system of a diode-clamped MMC with LA-PSC modulation to achieve sensorless operation while fully monitoring the modules' voltages per the protection and safety functions. The proposed estimator is very simple and needs no extra measurements at the modules, which can significantly reduce the number of sensors as well as the communication. The analysis and simulation results verify the feasibility and applicability of the proposed method. The simulation results confirm the estimator can achieve above 99%.

References

[1] N. Tashakor, F. Iraji, and S. G. Goetz, "Low-Frequency Scheduler for Optimal Conduction Loss in Series/Parallel Modular Multilevel Converters," *IEEE Transactions on Power Electronics,* pp. 1-1, 2021, doi: 10.1109/TPEL.2021.3110213.

[2] J. Fang, Z. Li, and S. M. Goetz, "Multilevel Converters With Symmetrical Half-Bridge Submodules and Sensorless Voltage Balance," *IEEE Transactions on Power Electronics,* vol. 36, no. 1, pp. 447-458, 2021, doi: 10.1109/TPEL.2020.3000469.

[3] J. Fang, H. Deng, N. Tashakor, F. Blaabjerg, and S. M. Goetz, "State-Space Modeling and Control of Grid-Tied Power Converters with Capacitive/Battery Energy Storage and Grid-Supportive Services," *IEEE Journal of Emerging and Selected Topics in Power Electronics,* pp. 1-1, 2021, doi: 10.1109/JESTPE.2021.3101527.

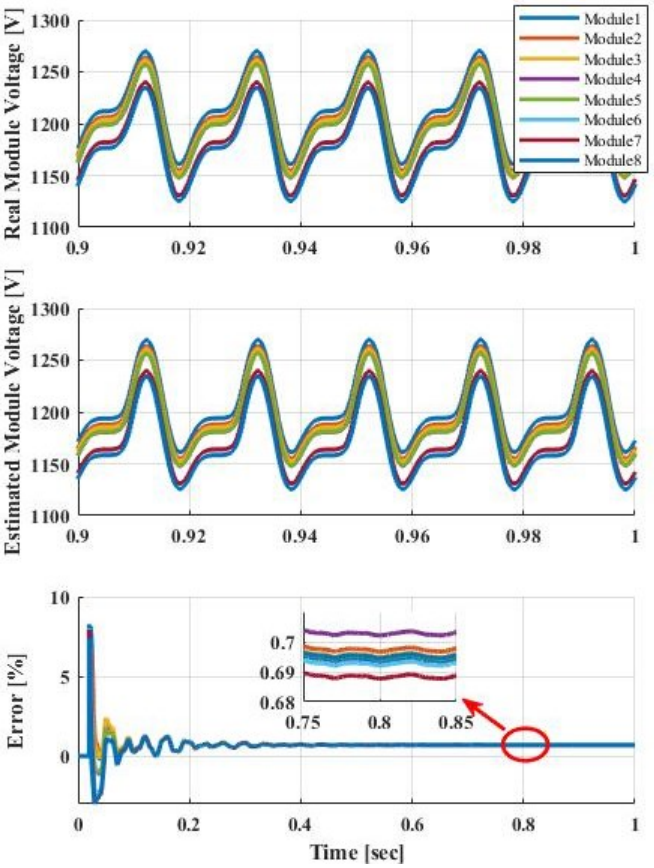

Fig. 7: Real and estimated modules' voltages and average error in balanced condition

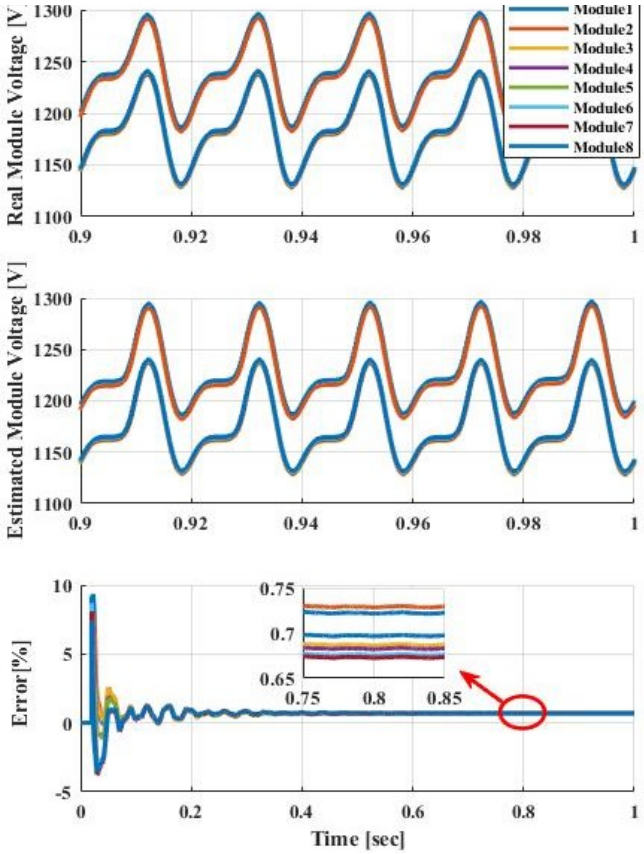

Fig. 8: Real and estimated modules' voltages and average error in unbalanced condition

[4] Q. Xiao, Y. Jin, and J. Wang, "A Novel Fault-Tolerant Control Method for Modular Multilevel Converter with an Improved Phase Disposition Level-Shifted PWM," *IEEE,* 2019.
[5] B. Arabsalmanabadi, N. Tashakor, Y. Zhang, K. Al-Haddad, and S. Goetz, "Parameter Estimation of Batteries in MMCs with Parallel Connectivity using PSO," presented at the IECON 2021 – 47th Annual Conference of the IEEE Industrial Electronics Society, 13-16 Oct. 2021, 2021.
[6] S. Ali, Z. Ling, K. Tian, and Z. Huang, "Recent Advancements in Submodule Topologies and Applications of MMC," *IEEE Journal of Emerging and Selected Topics in Power Electronics,* pp. 1-1, 2020, doi: 10.1109/JESTPE.2020.2990689.
[7] C. Wang, L. Xiao, C. Wang, M. Xin, and H. Jiang, "Analysis of the Unbalance Phenomenon Caused by the PWM Delay and Modulation Frequency Ratio Related to the CPS-PWM Strategy in an MMC System," *IEEE Transactions on Power Electronics,* vol. 34, no. 4, pp. 3067-3080, 2019, doi: 10.1109/TPEL.2018.2849088.
[8] J. Fang, S. Yang, H. Wang, N. Tashakor, and S. Goetz, "Reduction of MMC capacitances through parallelization of symmetrical half-bridge submodules," *IEEE Transactions on Power Electronics,* 2021.
[9] F. Deng, C. Liu, Q. Wang, R. Zhu, X. Cai, and Z. Chen, "A Currentless Submodule Individual Voltage Balancing Control for Modular Multilevel Converters," *IEEE Transactions on Industrial Electronics,* pp. 1-1, 2019, doi: 10.1109/TIE.2019.2952808.
[10] K. Wang, Y. Deng, H. Peng, G. Chen, G. Li, and X. He, "An Improved CPS-PWM Scheme-Based Voltage Balancing Strategy for MMC With Fundamental Frequency Sorting Algorithm," *IEEE Transactions on Industrial Electronics,* vol. 66, no. 3, pp. 2387-2397, 2019, doi: 10.1109/TIE.2018.2813963.
[11] T. Yin, Y. Wang, X. Wang, S. Yin, S. Sun, and G. Li, "Modular Multilevel Converter With Capacitor Voltage Self-balancing Using Reduced Number of Voltage Sensors," presented at the 2018 International Power Electronics Conference (IPEC-Niigata 2018 -ECCE Asia), 20-24 May 2018, 2018.
[12] P. Poblete, G. Pizarro, G. Droguett, F. Nunez, P. Judge, and J. Pereda, "Distributed Neural Network Observer for Submodule Capacitor Voltage Estimation in Modular Multilevel Converters," *IEEE Transactions on Power Electronics,* pp. 1-1, 2022, doi: 10.1109/TPEL.2022.3163395.
[13] G. Pizarro, P. M. Poblete, G. Droguett, J. Pereda, and F. Nunez, "Extended Kalman Filtering for Full State Estimation and Sensor Reduction in Modular Multilevel Converters," *IEEE Transactions on Industrial Electronics,* pp. 1-1, 2022, doi: 10.1109/TIE.2022.3165286.
[14] A. Dekka, B. Wu, and N. R. Zargari, "A Novel Modulation Scheme and Voltage Balancing Algorithm for Modular Multilevel Converter," *IEEE Transactions on Industry Applications,* vol. 52, no. 1, pp. 432-443, 2016, doi: 10.1109/TIA.2015.2477481.
[15] N. Tashakor, B. Arabsalmanabadi, F. Naseri, and S. Goetz, "Low-Cost Parameter Estimation Approach for Modular Converters and Reconfigurable Battery Systems Using Dual-Kalman-Filter," *IEEE Transactions on Power Electronics,* pp. 1-1, 2021, doi: 10.1109/TPEL.2021.3137879.
[16] P. Fang Zheng, "A generalized multilevel inverter topology with self voltage balancing," *IEEE Transactions on Industry Applications,* vol. 37, no. 2, pp. 611-618, 2001, doi: 10.1109/28.913728.
[17] N. Tashakor, Z. Li, and S. M. Goetz, "A Generic Scheduling Algorithm for Low-Frequency Switching in Modular Multilevel Converters with Parallel Functionality," *IEEE Transactions on Power Electronics,* pp. 1-1, 2020, doi: 10.1109/TPEL.2020.3018168.
[18] Z. Li, J. K. Motwani, Z. Zeng, S. Lukic, A. V. Peterchev, and S. Goetz, "A Reduced Series/Parallel Module for Cascade Multilevel Static Compensators Supporting Sensorless Balancing," *IEEE Transactions on Industrial Electronics,* pp. 1-1, 2020, doi: 10.1109/TIE.2020.2965470.
[19] X. Hu, Y. Zhu, J. Zhang, F. Deng, and Z. Chen, "Unipolar Double-Star Submodule for Modular Multilevel Converter With DC Fault Blocking Capability," *IEEE Access,* vol. 7, pp. 136094-136105, 2019, doi: 10.1109/ACCESS.2019.2942137.
[20] H. B. I, S. Rivera, Z. Li, S. Goetz, A. Peterchev, and R. L. F, "Different parallel connections generated by the Modular Multilevel Series/Parallel Converter: an overview," presented at the IECON 2019 - 45th Annual Conference of the IEEE Industrial Electronics Society, 14-17 Oct. 2019, 2019.
[21] M. B. Ghat and A. Shukla, "A New H-Bridge Hybrid Modular Converter (HBHMC) for HVDC Application: Operating Modes, Control, and Voltage Balancing," *IEEE Transactions on Power Electronics,* vol. 33, no. 8, pp. 6537-6554, 2018, doi: 10.1109/TPEL.2017.2751680.
[22] J. Xu, J. Li, J. Zhang, L. Shi, X. Jia, and C. Zhao, "Open-loop voltage balancing algorithm for two-port full-bridge MMC-HVDC system," *International Journal of Electrical Power & Energy Systems,* vol. 109, pp. 259-268, 2019/07/01/ 2019, doi: https://doi.org/10.1016/j.ijepes.2019.01.032.
[23] J. Rodriguez, L. Jih-Sheng, and P. Fang Zheng, "Multilevel inverters: a survey of topologies, controls, and applications," *IEEE Transactions on Industrial Electronics,* vol. 49, no. 4, pp. 724-738, 2002, doi: 10.1109/TIE.2002.801052.

[24] N. Tashakor, V. Monteiro, T. Ghanbari, and E. Farjah, "An Improved Modular Charge Equalization Structure for Series Cascaded Battery," presented at the 2019 27th Iranian Conference on Electrical Engineering (ICEE), 30 April-2 May 2019, 2019.

[25] J. Xu, J. Zhang, J. Li, L. Shi, X. Jia, and C. Zhao, "Series-parallel HBSM and two-port FBSM based hybrid MMC with local capacitor voltage self-balancing capability," *International Journal of Electrical Power & Energy Systems,* vol. 103, pp. 203-211, 2018.

[26] F. Z. Peng, W. Qian, and D. Cao, "Recent advances in multilevel converter/inverter topologies and applications," in *The 2010 International Power Electronics Conference - ECCE ASIA -*, 21-24 June 2010 2010, pp. 492-501, doi: 10.1109/IPEC.2010.5544625.

[27] C. Gao and J. Lv, "A new parallel-connected diode-clamped modular multilevel converter with voltage self-balancing," *IEEE Transactions on Power Delivery,* vol. 32, no. 3, pp. 1616-1625, 2017.

[28] N. Tashakor, M. Kilictas, J. Fang, and S. Goetz, "Switch-Clamped Modular Multilevel Converters with Sensorless Voltage Balancing Control," *IEEE Transactions on Industrial Electronics,* 2020.

[29] T. Zheng *et al.*, "A Novel High-Voltage DC Transformer Based on Diode-Clamped Modular Multilevel Converters With Voltage Self-Balancing Capability," *IEEE Transactions on Industrial Electronics,* vol. 67, no. 12, pp. 10304-10314, 2020, doi: 10.1109/TIE.2019.2962486.

[30] J. Fang, F. Blaabjerg, S. Liu, and S. Goetz, "A Review of Multilevel Converters with Parallel Connectivity," *IEEE Transactions on Power Electronics,* pp. 1-1, 2021, doi: 10.1109/TPEL.2021.3075211.

[31] G. Lu, C. Gao, and X. Li, "Voltage self-balance method for series connected IGBTs by using clamping diodes," presented at the IECON 2017 - 43rd Annual Conference of the IEEE Industrial Electronics Society, 29 Oct.-1 Nov. 2017, 2017.

[32] C. Gao, X. Jiang, Y. Li, Z. Chen, and J. Liu, "A DC-Link Voltage Self-Balance Method for a Diode-Clamped Modular Multilevel Converter With Minimum Number of Voltage Sensors," *IEEE Transactions on Power Electronics,* vol. 28, no. 5, pp. 2125-2139, 2013, doi: 10.1109/TPEL.2012.2212915.

[33] J. Xu, M. Feng, H. Liu, S. Li, X. Xiong, and C. Zhao, "The diode-clamped half-bridge MMC structure with internal spontaneous capacitor voltage parallel-balancing behaviors," *International Journal of Electrical Power & Energy Systems,* vol. 100, pp. 139-151, 2018.

[34] X. Liu *et al.*, "A Novel Diode-Clamped Modular Multilevel Converter With Simplified Capacitor Voltage-Balancing Control," *IEEE Transactions on Industrial Electronics,* vol. 64, no. 11, pp. 8843-8854, 2017, doi: 10.1109/TIE.2017.2682013.

[35] T. Zheng, C. Gao, X. Liao, X. Liu, B. Sun, and J. Lv, "A medium-voltage motor drive based on diode-clamped modular multilevel converters," presented at the 2017 20th International Conference on Electrical Machines and Systems (ICEMS), 11-14 Aug. 2017, 2017.

[36] N. Tashakor, M. Kilictas, E. Bagheri, and S. Goetz, "Modular Multilevel Converter with Sensorless Diode-Clamped Balancing through Level-Adjusted Phase-Shifted Modulation," *IEEE Transactions on Power Electronics,* pp. 1-1, 2020, doi: 10.1109/TPEL.2020.3041599.

[37] H. Givi, E. Hosseini, and E. Farjah, "Estimation of Batteries Voltages and Resistances in Modular Multilevel Converter With Half-Bridge Modules Using Modified PSO Algorithm," presented at the 2021 12th Power Electronics, Drive Systems, and Technologies Conference (PEDSTC), 2-4 Feb. 2021, 2021.

[38] R. Chakraborty, J. Samantaray, A. Dey, and S. Chakrabarty, "Capacitor Voltage Estimation of MMC using a Discrete-Time Sliding Mode Observer Based on Discrete Model Approach," *IEEE Transactions on Industry Applications,* pp. 1-1, 2021, doi: 10.1109/TIA.2021.3124982.

[39] Z. Wang and L. Peng, "Grouping Capacitor Voltage Estimation and Fault Diagnosis With Capacitance Self-Updating in Modular Multilevel Converters," *IEEE Transactions on Power Electronics,* vol. 36, no. 2, pp. 1532-1543, 2021, doi: 10.1109/TPEL.2020.3011131.

[40] Z. Ke *et al.*, "Capacitor Voltage Ripple Estimation and Optimal Sizing of Modular Multi-Level Converters for Variable-Speed Drives," *IEEE Transactions on Power Electronics,* vol. 35, no. 11, pp. 12544-12554, 2020.

[41] B. Arabsalmanabadi, N. Tashakor, S. Goetz, and K. Al-Haddad, "Li-ion Battery Models and A Simplified Online Technique to Identify Parameters of Electric Equivalent Circuit Model for EV Applications," presented at the IECON 2020 The 46th Annual Conference of the IEEE Industrial Electronics Society, 18-21 Oct. 2020, 2020.

[42] Y. Jin *et al.*, "A Novel Submodule Voltage Balancing Scheme for Modular Multilevel Cascade Converter—Double-Star Chopper-Cells (MMCC-DSCC) based STATCOM," *IEEE Access,* 2019.